Appendix A: Detailed period-spacing pattern plots

Appendix B: Tight R constraint

Appendix C: Other frequency groups

The focus of this work has been asteroseismic exploitation of a dipole prograde gravito-inertial mode period-spacing pattern. However, there are some additional smaller groups of frequencies within the Fourier spectrum. Here, we briefly describe these features and speculate on their potential utility in the context of future, more refined modelling attempts.

Between 0.1 d and 0.28 d in the periodogram, there are a large number of statistically significant periods where we expect quadrupole and septupole series to appear (around 0.14 d and 0.2 d, respectively). There is a great deal of contamination, however, and only a few consecutive periods in a (probable) quadrupole pattern can be identified. The relevant extracted frequencies are shown in Fig. C.1. These series did not feature as part of our analysis, the main component of which relied on asteroseismic models of prograde dipole modes.

As previously noted by Hełminiak et al. (2017), there are several low-frequency cones present in the Fourier spectrum around 0.19 d^{-1}, 0.38 d^{-1}, and 0.56 d^{-1}, with the two higher frequency cones presumably being harmonics relating to the dominant 0.19 d^{-1} cone. These cones are shown in Figure C.2. Hełminiak et al. (2017) propose that the 0.18 d^{-1} is caused by rotation one or both of the two G stars Ba and Bb, commenting that the complicated structure of these peaks could be a result of either differential rotation or originate from two stars rotating at similar rates. From atmospheric modelling of the disentangled spectra in Kemp et al. (2024), the rotation rates for Ba and Bb were estimated to be $v$sin(i)=8.9 ± 1.1 km s^{-1} and $v$sin(i)=9.2 ± 1.1 km s^{-1}, respectively. From Hełminiak et al. (2017), we also have estimates for the stellar radii for the Ba and Bb of 0.888 ± 0.010 $R_\odot$ and 0.856 ± 0.038 $R_\odot$, respectively. Assuming rigid rotation, this corresponds to rotation frequencies of approximately 0.2 ± 0.02 d^{-1} and 0.21 ± 0.03 d^{-1}. This is slightly higher than expected from the centre of the cone, although within uncertainty. It is likely that even a small systematic error in either the rotation velocity or the radius estimate could resolve this. We note that in the scenario of differential rotation, an offset between the surface rotation and the interior might be expected. However, according to our surface rotation estimate the surface would be rotating slightly faster than the interior, and significantly faster than the orbital frequency of the eccentric B binary (0.116 d^{-1}). We conclude that the rotation of the B stars is almost certainly the cause of these cones, noting that the surface rotation rate is consistent with the cone frequencies to within $1-\sigma$.

Finally, there are the high-amplitude p-modes at 17.75 d^{-1}, 18.48 d^{-1}, 20.24 d^{-1}, and 22.62 d^{-1}(see Fig. 4). They exhibit significant, symmetric splitting that is present after prewhitening. The splitting corresponds to the orbital frequency of the Aa binary, and may be due to light travel-time effects. Similar splittings are only occasionally visible in the g-mode regime, but are but are never statistically significant even for the high-amplitude peaks. There is no sign of rotational splitting.

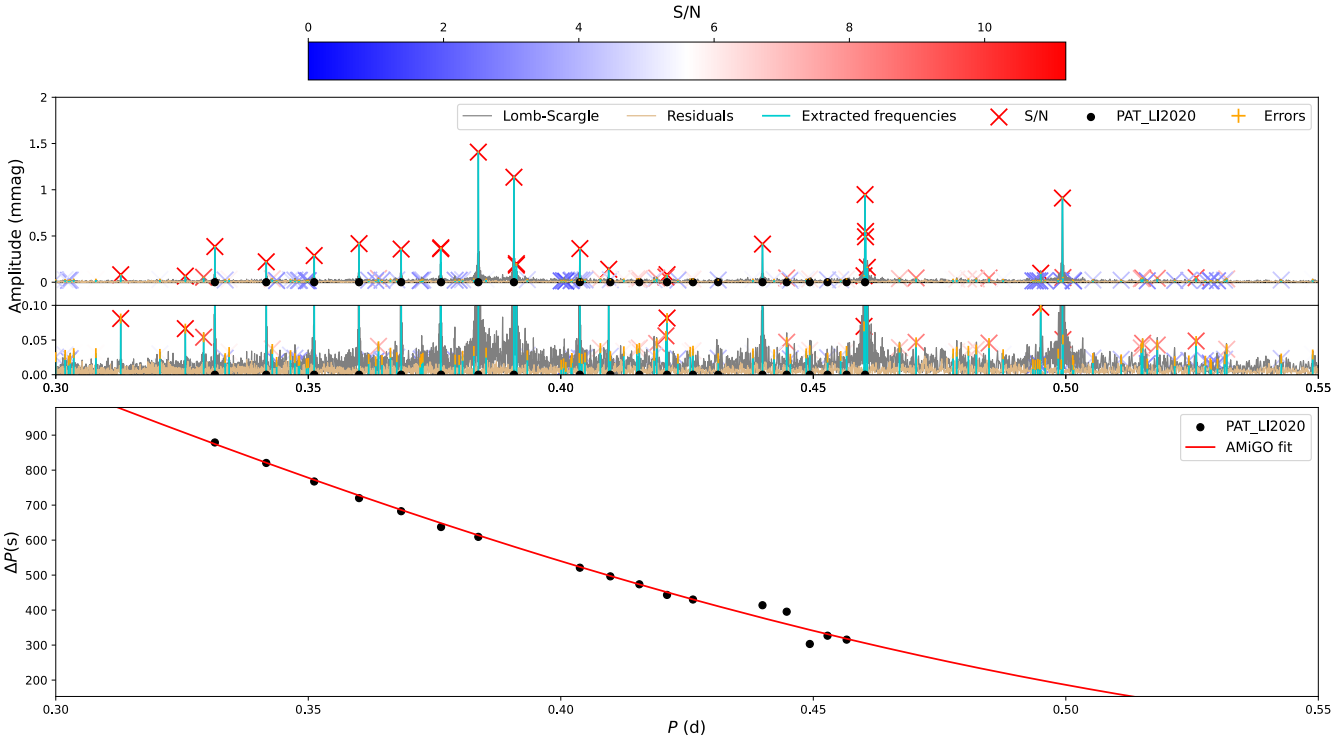

Fig. A.1: PAT_LI2020 period-spacing pattern from Li et al. (2020a). The Lomb-Scargle periodogram is shown in grey, the extracted frequencies in light blue, and the residual periodogram with the extracted frequencies removed in orange. Orbital harmonics are excluded. The SNR ratio is indicated by the colour of the 'X' symbol for each extracted frequency, while the amplitude and period errors (more easily seen in the inset panel, which better shows the low-amplitude behaviour) are shown in orange. The extracted frequencies selected to be part of the pattern are marked with a filled black circle. Note that only the black point and the AMiGO fit and predictions are specifically related to the PAT_LI2020 pattern; the Lomb-Scargle periodogram and its residuals, as well as the extracted frequencies (and their associated SNR and errors), are included from the period04 extraction for comparison purposes.

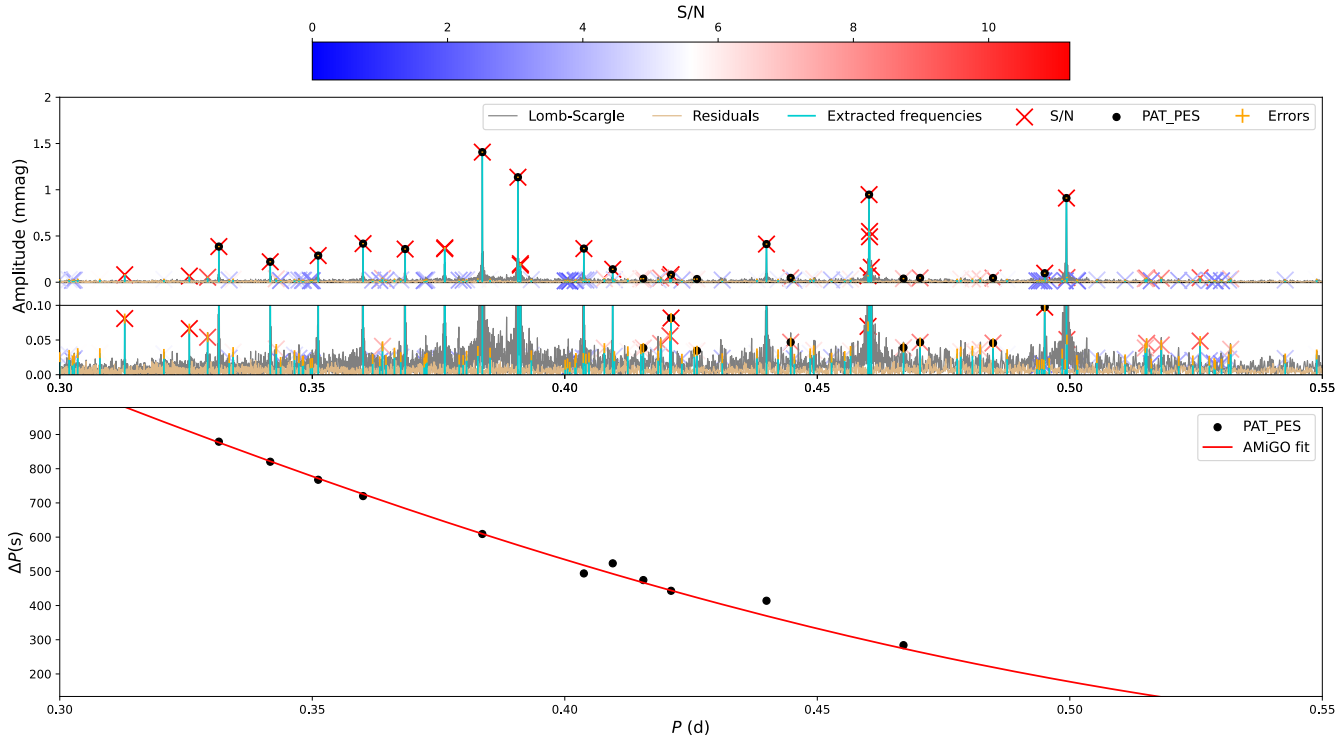

Fig. A.2: PAT_P04_PES period-spacing pattern. Orbital harmonics are excluded. The high-amplitude period at 0.36d is excluded in this pattern only due to its near-perfect coincidence with an 8.65d orbital harmonic. A detailed description of all symbols and information can be found in Figure A.1.

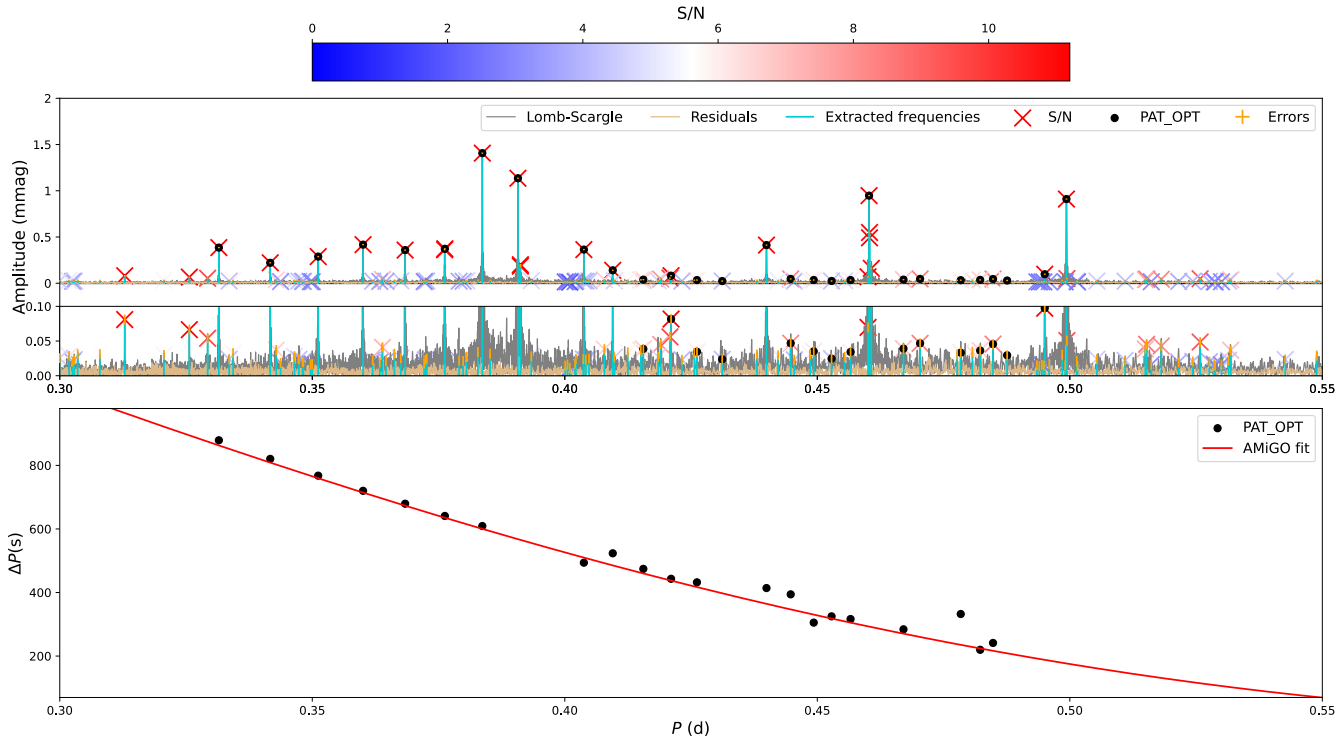

Fig. A.3: PAT_P04_OPT period-spacing pattern. Orbital harmonics are excluded. A detailed description of all symbols and information can be found in Figure A.1.

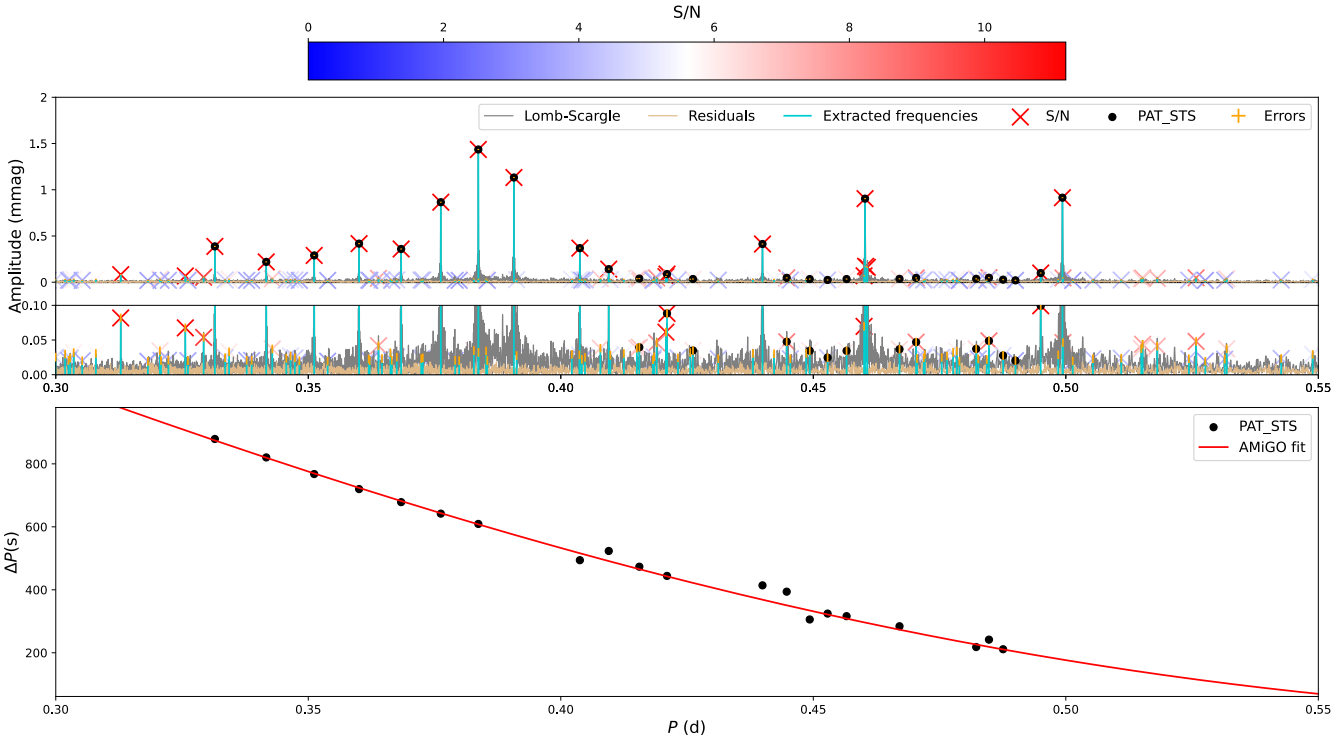

Fig. A.4: PAT_STS period-spacing pattern. Orbital harmonics are excluded. A detailed description of all symbols and information can be found in Figure A.1.

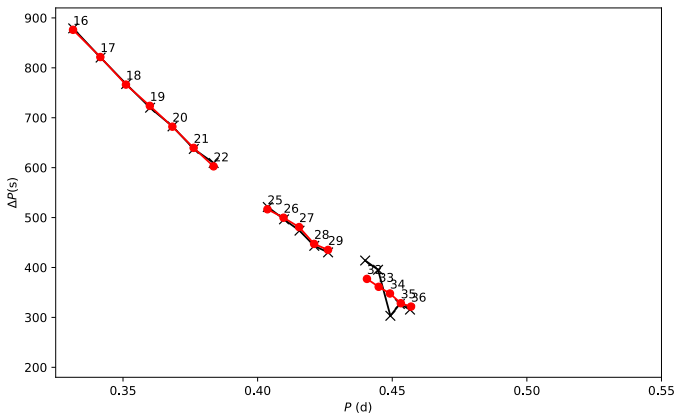

(a) PAT_LI2020

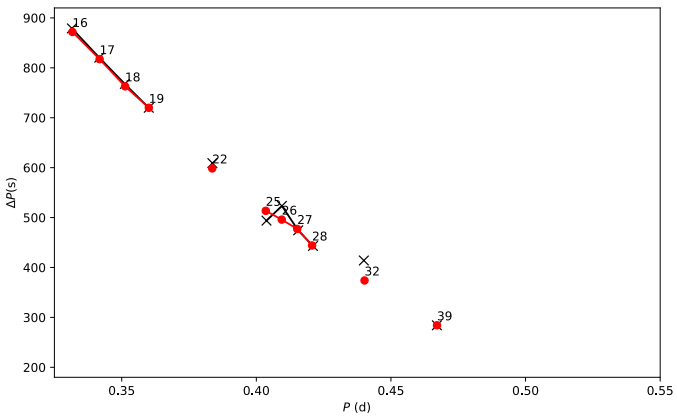

(b) PAT_P04_PES

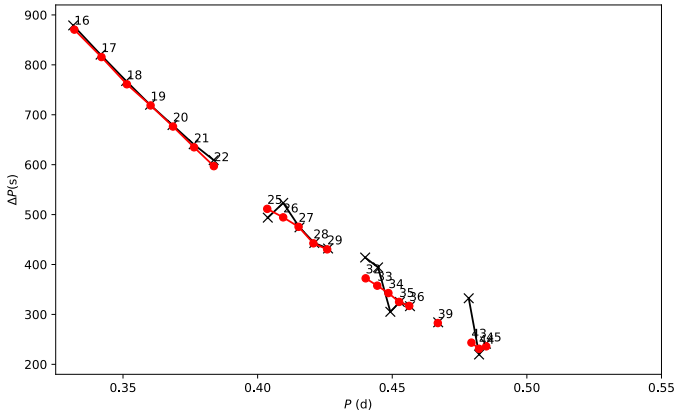

(c) PAT_P04_OPT

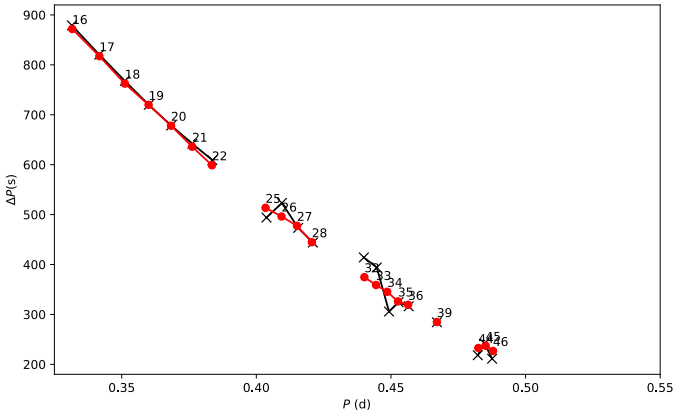

(d) PAT_STS

Fig. B.1: Best-fitting C-3PO models (red) consistent with the tight and spectroscopic constraints from the high resolution sampling. Observed patterns are shown in black.

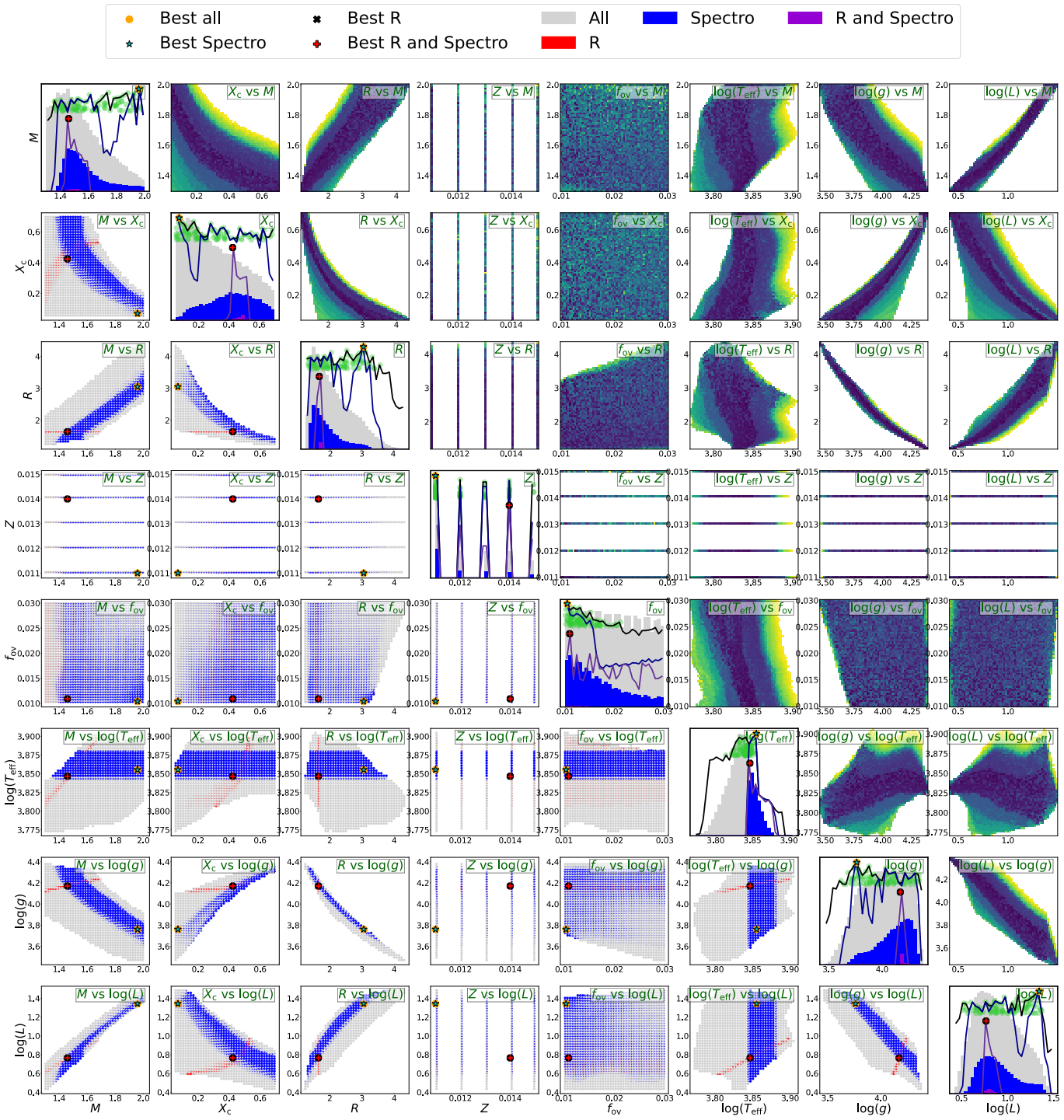

Fig. B.2: PAT_LI2020 PAT_P04_PES modelling results, tight radial constraint. See Fig. 8 for detailed description of the different plot elements.

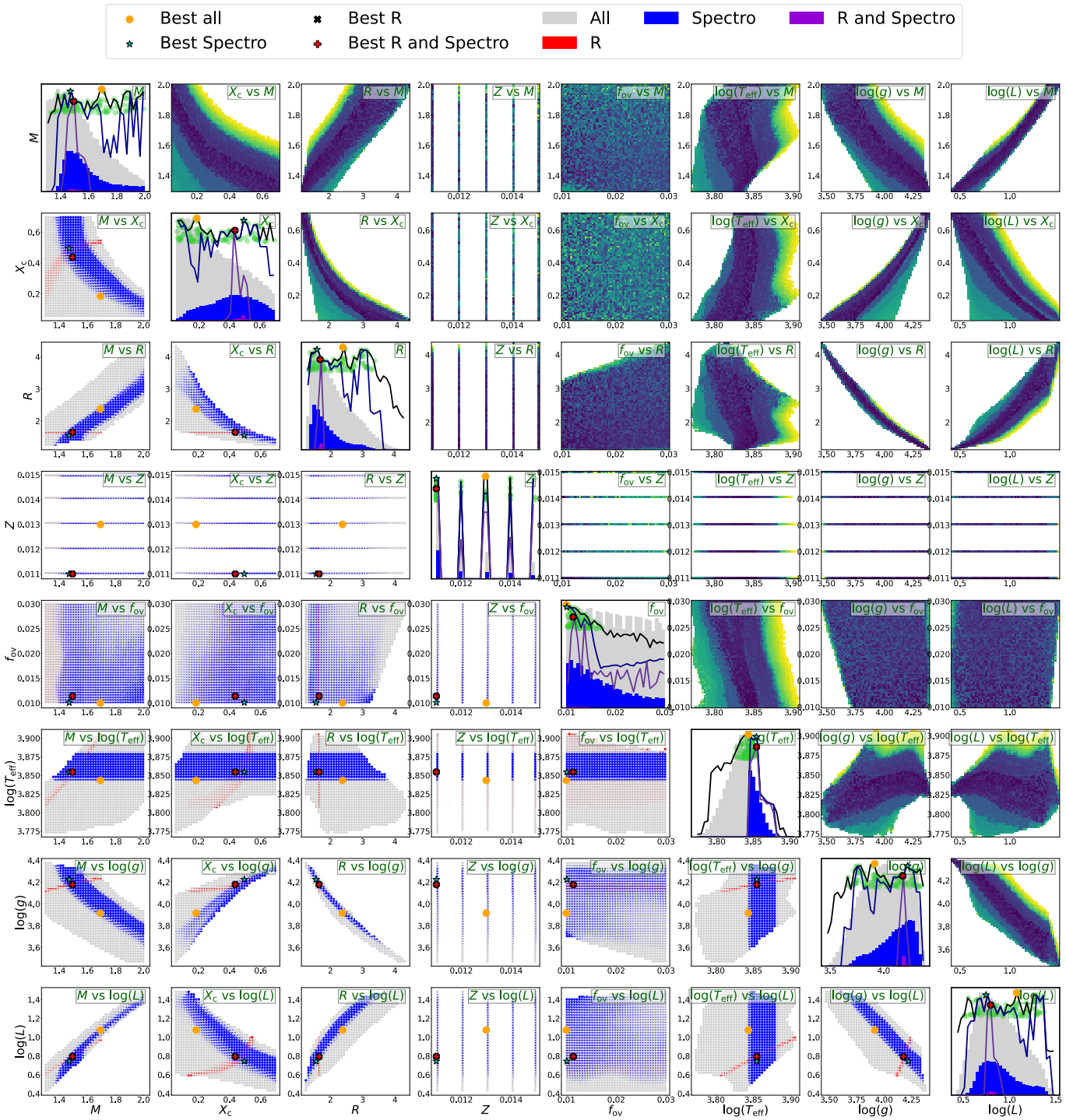

Fig. B.3: PAT_P04_PES modelling results, tight radial constraint. See Fig. 8 for detailed description of the different plot elements.

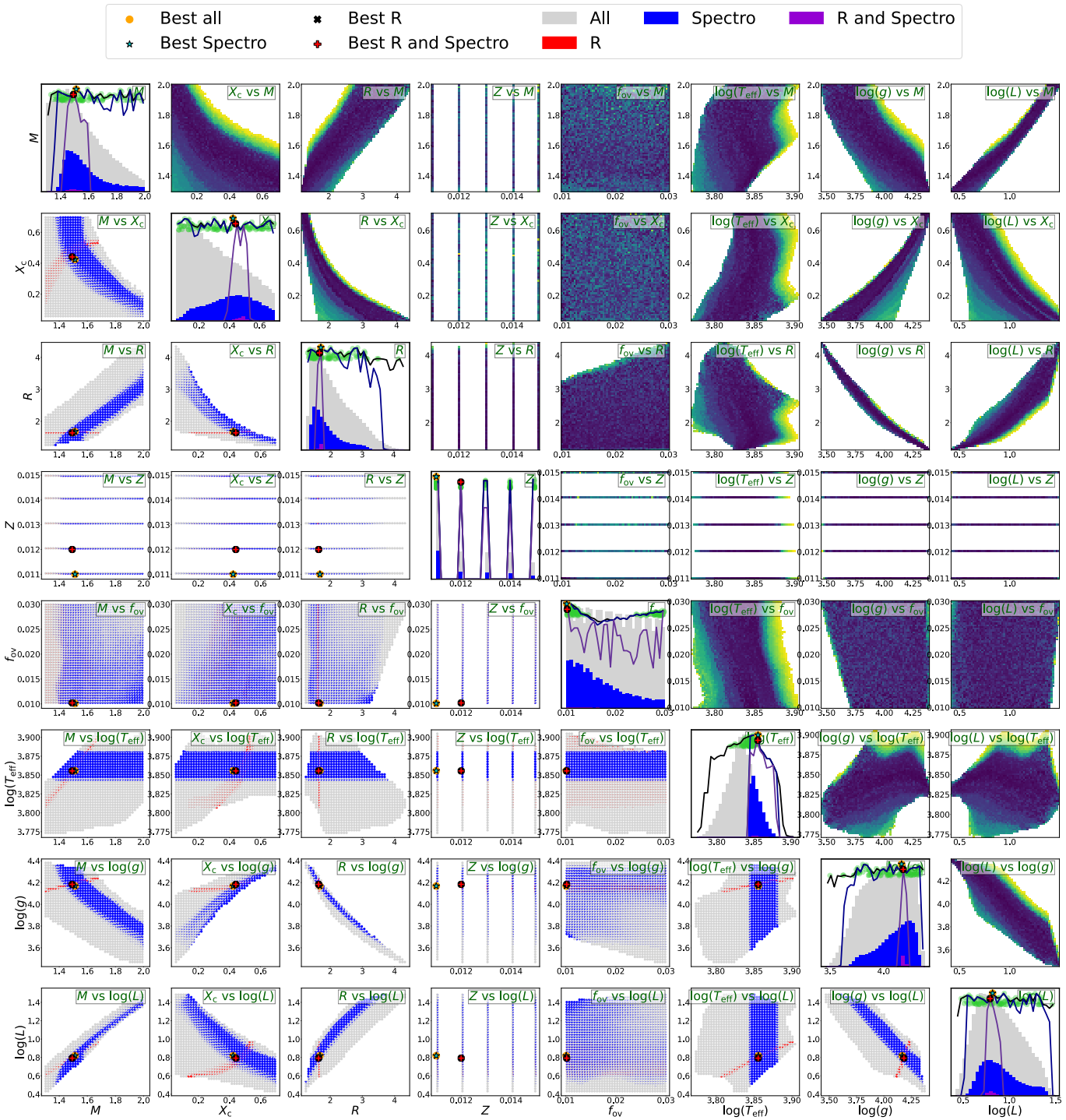

Fig. B.4: PAT_P04_OPT modelling results, tight radial constraint. See Fig. 8 for detailed description of the different plot elements.

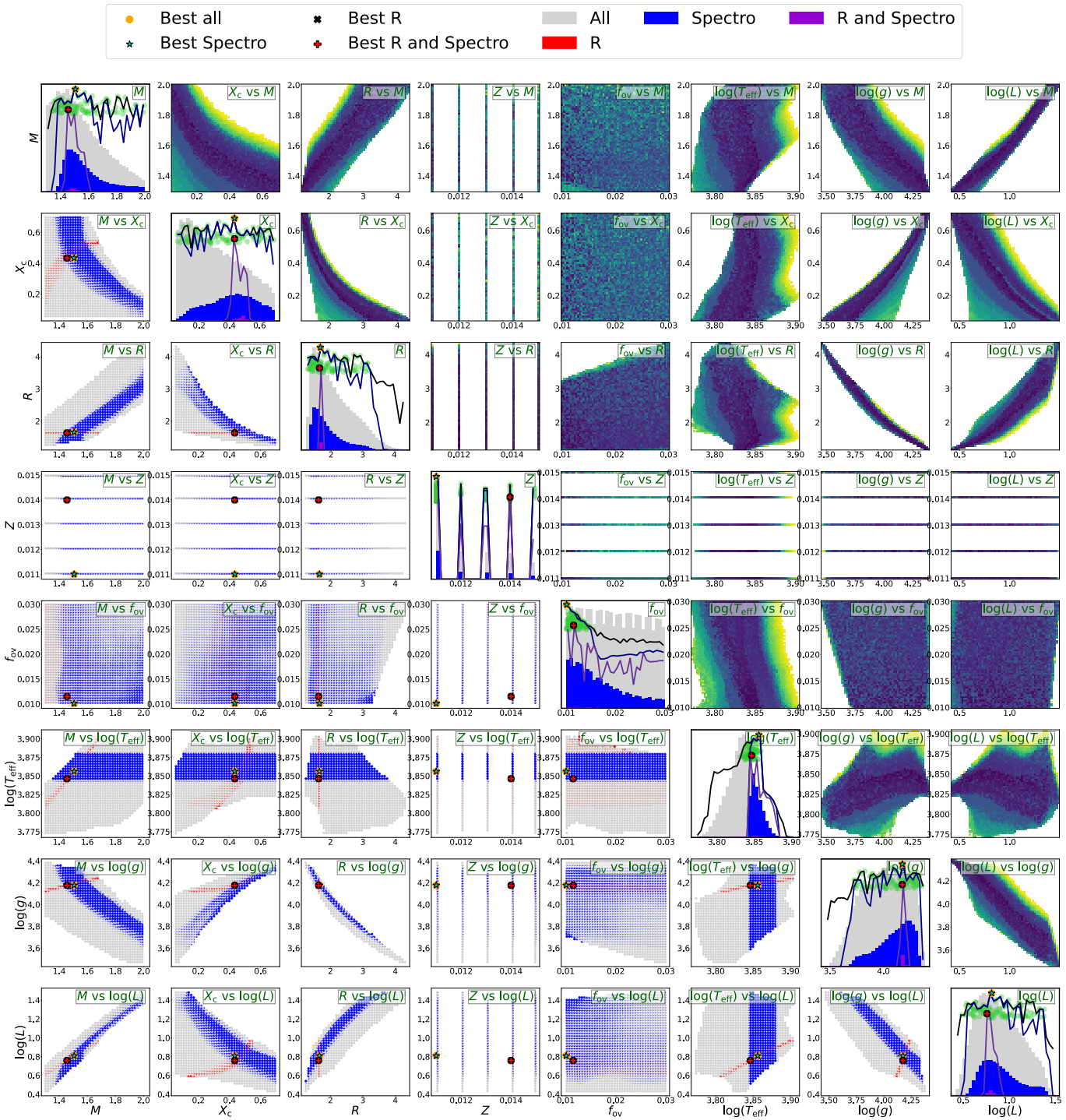

Fig. B.5: PAT_STS modelling results, tight radial constraint. See Fig. 8 for detailed description of the different plot elements.

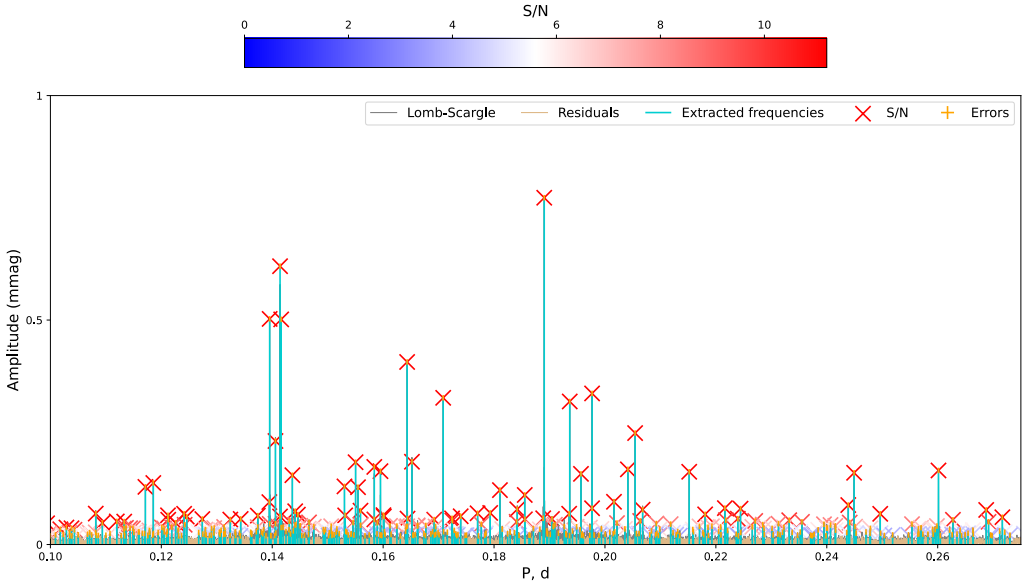

Fig. C.1: Likely high order g-modes, shown in the period domain. The cluster around 0.2 d are where we expect the l=2 series to appear, while those around 0.14 are likely the l=3 series. At most, a very short (perhaps 2-3 consecutive spacings) might be confidently obtained from the $l = 2$ series.

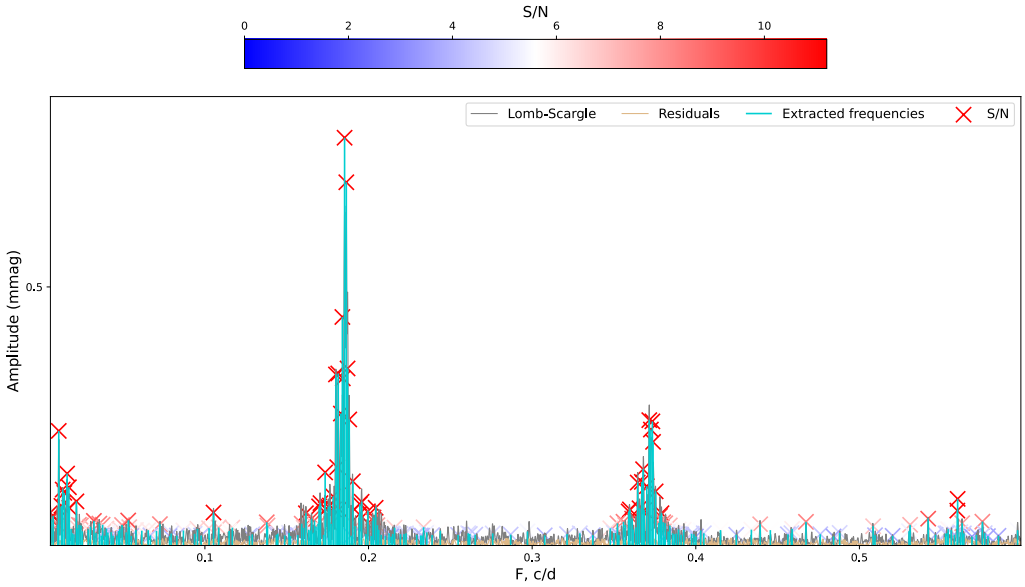

Fig. C.2: Series of low-frequency cones around 0.19, 0.38, and 0.56 d^{-1}. Origin of these frequency cones is unknown, and does not appear to coincide with any of the existing periods or known rotation rates.